


## Article

# Effective Removal of Refractory Pollutants through Cinnamic Acid-Modified Wheat Husk Biochar: Experimental and DFT-Based Analysis

Umme Habiba <sup>1</sup>, Sadaf Mutahir <sup>1,2,\*</sup>, Muhammad Asim Khan <sup>1,2,\*</sup> , Muhammad Humayun <sup>3</sup> ,  
Moamen S. Refat <sup>4</sup>  and Khurram Shahzad Munawar <sup>5</sup> 

<sup>1</sup> Department of Chemistry, University of Sialkot, Sialkot 51300, Pakistan

<sup>2</sup> School of Chemistry and Chemical Engineering, Linyi University, Linyi 276000, China

<sup>3</sup> Wuhan National Laboratory for Optoelectronics, School of Optical and Electronics Information, Huazhong University of Science and Technology, Wuhan 430074, China

<sup>4</sup> Department of Chemistry, College of Science, Taif University, Taif 21944, Saudi Arabia

<sup>5</sup> Department of Chemistry, University of Mianwali, Mianwali 42200, Pakistan

\* Correspondence: sadafmutahir@hotmail.com (S.M.); khanabdali@hotmail.com (M.A.K.)

**Abstract:** The removal of refractory pollutants, i.e., methylene blue (MB) and ciprofloxacin (CIP), relies heavily on sorption technologies to address global demands for ongoing access to clean water. Because of the poor adsorbent–pollutant contact, traditional sorption procedures are inefficient. To accomplish this, a wheat husk biochar (WHB), loaded with cinnamic acid, was created using a simple intercalation approach to collect dangerous organic pollutants from an aqueous solution. Batch experiments, detecting technologies, and density functional theory (DFT) calculations were used to investigate the interactions at the wheat husk biochar modified with cinnamic acid (WHB/CA) and water interface to learn more about the removal mechanisms. With MB (96.52%) and CIP (94.03%), the functionalized WHB exhibited outstanding adsorption capabilities, with model fitting results revealing that the adsorption process was chemisorption and monolayer contact. Furthermore, DFT studies were performed to evaluate the interfacial interaction between MB and CIP with the WHB/CA surface. The orbital interaction diagram provided a visual representation of the interaction mechanism. These findings open up a new avenue for researchers to better understand adsorption behavior for the utilization of WHB on an industrial scale.

**Keywords:** wheat husk biochar; cinnamic acid; wastewater treatment; adsorption; DFT



**Citation:** Habiba, U.; Mutahir, S.; Khan, M.A.; Humayun, M.; Refat, M.S.; Munawar, K.S. Effective Removal of Refractory Pollutants through Cinnamic Acid-Modified Wheat Husk Biochar: Experimental and DFT-Based Analysis. *Catalysts* **2022**, *12*, 1063. <https://doi.org/10.3390/catal12091063>

Academic Editor: Meng Li

Received: 21 August 2022

Accepted: 14 September 2022

Published: 17 September 2022

**Publisher's Note:** MDPI stays neutral with regard to jurisdictional claims in published maps and institutional affiliations.



**Copyright:** © 2022 by the authors. Licensee MDPI, Basel, Switzerland. This article is an open access article distributed under the terms and conditions of the Creative Commons Attribution (CC BY) license (<https://creativecommons.org/licenses/by/4.0/>).

## 1. Introduction

Rapid industrialization and massive growth in the human population have resulted in major environmental contamination in the last few decades. Increased concentrations of a wide variety of contaminants or pollutants, such as toxic heavy metal ions, inorganic anions, micropollutants, and organic compounds such as dyes, phenols, pesticides, humic substances, detergents, and other persistent organic pollutants, have been widely reported in recent decades in various parts of the world. The release of these harmful chemicals into natural water bodies has devastated flora and fauna and has disrupted the ecological balance. Many of these pollutants are not only chemically or biologically resistant, but they also have a high level of environmental mobility and a high potential for bioaccumulation in the food chain [1]. Water contaminants include inorganic dangerous elements, organic compounds, and microorganisms. Inorganic hazardous elements include mercury, cadmium, lead, chromium, copper, and other inorganic metallic elements. Common organic contaminants in water include pharmaceuticals, personal care products, endocrine disruptors, pesticides, organic dyes, detergents, and common industrial organic wastes, such as phenolics, halogens, and aromatics [2–4].

Dyes are an important class of aromatic hydrocarbons that pollute the environment. These are colored substances used in various industries [5]. Each year, 5–10% of the  $7 \times 10^5$  metric tons of dyes produced are discharged as waste into water [6]. Although these are used in a variety of industries for a variety of purposes, their presence in water is extremely hazardous due to their poor degradability, unpleasant odor, high toxicity level, and retardation of light penetration into the water, causing the photosynthesis process to halt, thereby disrupting the entire ecosystem [7].

There are various classes of dyes; among these, methylene blue is an important dye. It is a heterocyclic compound with the chemical formula  $C_{16}H_{18}N_3SCl \cdot 3H_2O$ . Methylene blue (MB), a biological staining agent, is the most commonly used cationic dye in the wool, silk, leather, calico, cotton, and tannin industries. MB, which can inflict eye burns on humans and aquatic critters and permanently harm their eyes. Furthermore, depending on the length of time that people are exposed to MB, it can be hazardous to their health. Long-term MB exposure can result in a burning sensation, mental disorientation, nausea, vomiting, methemoglobinemia, cyanosis, convulsions, dyspnea, anemia, and hypertension, whereas short-term exposure might result in quick or difficult breathing [8–10].

Ciprofloxacin is a second-generation fluoroquinolone antibiotic that targets Gram-negative and Gram-positive bacteria and has a fluorine atom at position 6 in the quinoline group. Its superior properties, such as excellent tissue penetration, good bioavailability, and fewer side effects, led doctors and veterinarians all over the world to prescribe it to treat a variety of bacterial infections, including infections of the respiratory system, skin, bone, joints, urinary tract, and gastrointestinal tract [11]. According to many studies from around the world, ciprofloxacin has been identified in alarming proportions in a range of environmental systems, including agricultural soils, groundwater, surface water, and effluents from various wastewater treatment plants (i.e., domestic, hospital, and industrial) [12,13]. Even though ciprofloxacin concentrations in aquatic environments range from  $ngL^{-1}$  to  $gL^{-1}$ , these levels are adequate to cause and accelerate antimicrobial resistance gene (AMR) proliferation in water. These genes can infect the body (human or animal) with fatal diseases, while tolerating or competing with any antibiotic, posing a severe threat to the world's limited water supply. If reasonable measures to lower ciprofloxacin content and related resistant genes in water are not performed, AMRs could become a future pandemic similar to COVID-19 [14].

As a result, contaminated water and wastewater must be cleaned before being discharged into the natural environment. To remove organic contaminants from wastewater, many approaches have been tried, including electrochemical treatment [15], biological treatment [16], photodegradation [17], ozonation [18], electrochemical treatment [19], membrane filtration, oxidation [20], adsorption [21], reverse osmosis [22], physical nanofiltration [23,24], chemical oxidation [25,26], ion exchange, and electrocoagulation [27]. Among these methods, adsorption is considered one of the best methods, because it is low-cost, the nontoxic adsorbent can be regenerated, it is easy to operate, and has no chance of high toxicity [28]. However, the surface area, porosity, and pore diameter of the adsorbent and adsorbate that are utilized determine the efficacy of the adsorption process. This approach has used a variety of adsorbents, including carbon-based adsorbents [29], polymers and resins [30,31], metal-organic frameworks, clays and minerals [32,33], nanomaterials [34] [35,36] such as PTA/Zr-MCM-41, and metals and their oxides [37], which have been used for the adsorption of antibiotics/dyes. Activated carbon is the most important and frequently used cost-effective adsorbent; it can be regenerated with some mass loss. The production of activated carbon from different sources results in a difference in porosity, adsorption, and other properties. Moreover, the method of preparation of activated carbon and parameters used during this method affect the acidic and basic nature of activated carbon [38].

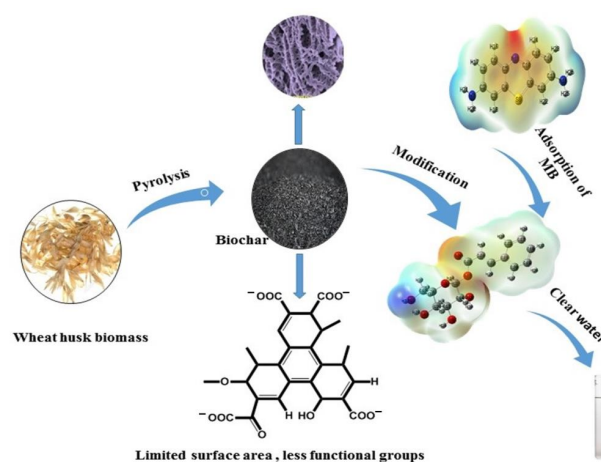
One of the serious problems is that the direct usage of these adsorbents creates many problems, such as poor adsorption capacity, emission of secondary pollutants, high COD, BOD, and TOC [39], while wheat husk biochar modified with cinnamic acid has no such

problems. It does not create sludge formation, nor does it emit secondary pollutants, and it has no effects on BOD, COD, or TOC.

Biochar derived from wheat husk can be used as an adsorbent because it has a high surface area, insolubility in water, high mechanical strength, and various functional groups. Moreover, it has some alkali metal content that also enhances its adsorption capacity. The chemical composition of wheat husk includes cellulose, 33.7–40%; hemicellulose, 21–26%; lignin, 11–22.9%; and extractives that include alkali metal contents and silica, which account for 15.3% [40].

Tons of wheat husk are produced every year, with very little usage in feedstock, energy production, and the adsorption process. A large amount of wheat husk is thrown out as waste material. The use of wheat husk as an adsorbent for the removal of organic pollutants not only provides a solution for the usage of this waste material in a useful form, but also plays an effective role in wastewater treatment. It is the cheapest and most renewable source, but the problem is that natural wheat husk exhibits very poor adsorption capacity. Although wheat straw biochar has been reported in the literature for the removal of MB, it has a very low adsorption capacity of 46.6 mg/g in the absence of a magnetic field, and 62.5 mg/g in the presence of a magnetic field. This poor adsorption capacity is not sufficient for today's threatening levels of pollutants [41]. Other modification techniques can be used to improve the properties of the wheat husk [42]. The modification increases surface area and adsorption properties [43].

This paper reports the modification of wheat husk-derived biochar with cinnamic acid, as it is not a harsh acid, is less toxic, and is environmentally friendly, while the previously reported modifying agents are harsh and have some toxic effects. There is currently no literature available on the adsorption of organic pollutants using cinnamic acid-modified wheat husk biochar. A study has been carried out on wheat husk biochar that has very little affinity toward the removal of MB only, but no study has been carried out on wheat husk biochar loaded with cinnamic acid for the removal of antibiotics. As a result, the goal of this study was to fill a research gap by analyzing organic pollutant removal utilizing cinnamic acid-modified wheat husk biochar and batch adsorption. Methylene blue, a well-known thiazine dye, was chosen to represent cationic dyes, while ciprofloxacin, a fluoroquinolone antibiotic with a fluorine atom at position 6 in the quinoline group, was chosen to represent non-cationic colors. As part of the research, the adsorbent was characterized based on its surface appearance and pore characteristics. In batch mode, the impacts of key adsorption factors, such as adsorbent dosage, beginning pH, contact time, and initial concentration, were also investigated. Finally, the adsorption mechanisms on both MB and ciprofloxacin, with cinnamic acid-modified wheat husk biochar as the adsorbent, were investigated using the fitting of experimental data with adsorption equilibrium isotherm, kinetic, and mechanism models, as well as theoretical studies (Scheme 1).



**Scheme 1.** Schematic representation of modified wheat husk-based wastewater treatment.

Hence, this study signifies that by preparing WHB/CA, we can remove refractory pollutants from wastewater in heavy amounts. So, we can not only overcome water pollution, but also land pollution.

## 2. Results and Discussion

### 2.1. SEM Analysis

The adsorbent's surface micromorphology has a significant impact on its adsorption performance. The micromorphology of biochar may be seen easily and intuitively using scanning electron microscopy. The morphological changes of materials before and after alteration can be better examined using electron microscopy. Figure 1 shows the SEM-EDS pictures of the biochar before and after modification. The micromorphology of both WHB and 7.5%WHB/CA is an inhomogeneous porous structure with a roughened surface, as seen by SEM images (Figure 1). It can be seen from Figure 1a that the surface of WHB has many prominent cracks that are lessened in the surface of 7.5%WHB/CA (Figure 1b), and macropores are converted into microspores. Hence, the modifier aggregated on the surface of WHB, which is very effective for the adsorption of organic pollutants on its surface, while it is shown in Figure 1c that the surface of WHB has a small amount of debris on its surface, with some smoother contents, while the surface of the 7.5%WHB/CA (Figure 1d) is rough and was fully covered with the modifier. This aggregation on the surface of 7.5%WHB/CA was an indication of successful modification [44].

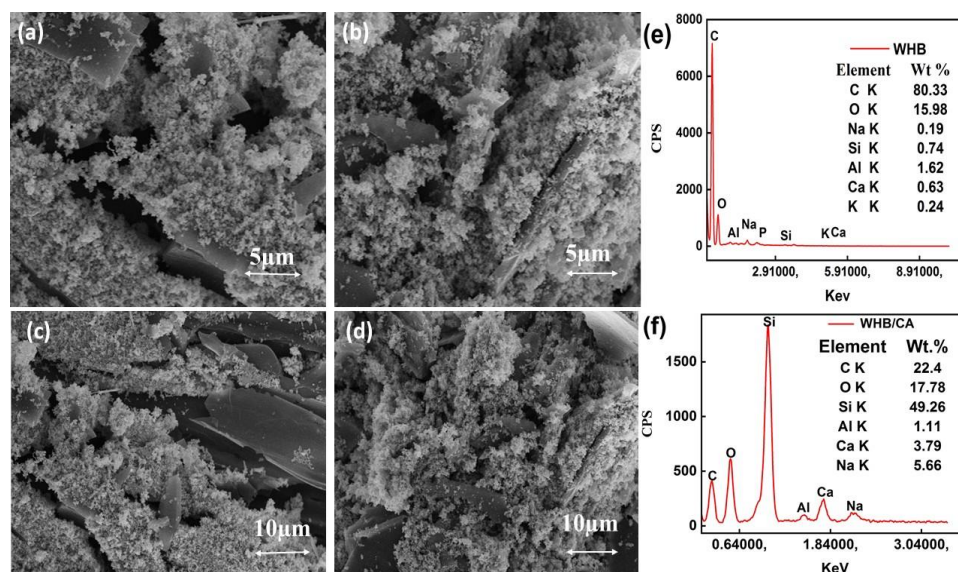


**Figure 1.** SEM of WHB (a,c) and WHB/CA (b,d), EDS of WHB (e), and EDS of MWH/CA (f).

### 2.2. XRD Analysis

XRD analysis was performed to investigate the crystallinity of the material. As shown in Figure 2, a characteristic peak at around  $22^\circ$  appeared, which corresponded to cellulose for WHB, while the same diffraction for 7.5%WHB/CA was very sharp, which is an indication of preferred orientation. It shows the removal of amorphous constituents, such as lignin and hemicellulose, and the insertion of cinnamic acid into the layers of WHB [45].

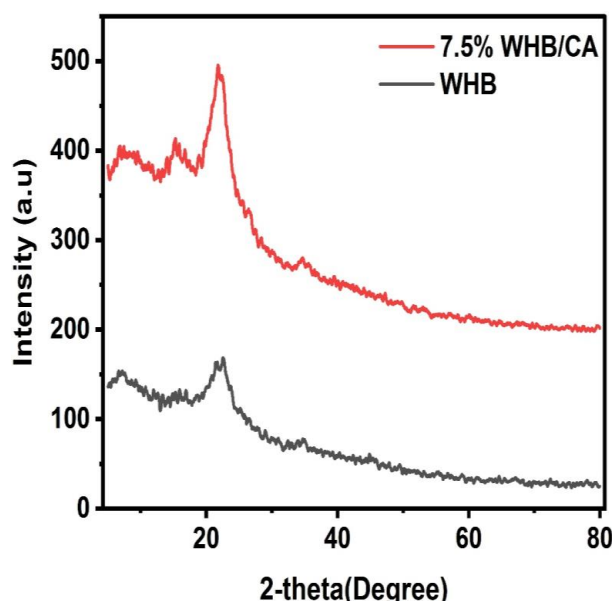


Figure 2. XRD of WHB and 7.5%WHB/CA.

### 2.3. FTIR Analysis

FTIR spectra of WHB, WHB/CA, and MB-WHB/CA samples were analyzed (Figure 3). The peak at  $2350\text{ cm}^{-1}$  gives evidence of CH stretch, and a peak at  $1640\text{ cm}^{-1}$  corresponded to the C=C of the aromatic ring [46]. The vibrations of the carboxylate (COO-) group were represented by a peak at  $1450\text{ cm}^{-1}$ , whereas the OCC stretch of the acetate group was represented by a peak at  $1160\text{ cm}^{-1}$ , indicating that WHB was esterified. The intensity of both peaks (C=O and COO-) increased after modification, which indicates that modification was performed, and some sort of rearrangement may have been performed in the biochar [47]. A band at  $1070\text{ cm}^{-1}$  was due to COC stretch [46], which was suppressed in the treated WH sample. Furthermore, the broadening of the peak at  $1160\text{ cm}^{-1}$  and the broadband of hydrogen-bonded OH at  $3400\text{ cm}^{-1}$  also indicates the adsorption of dye onto the modified sample. Hence, it is inferred that WHB/CA can adsorb MB effectively.

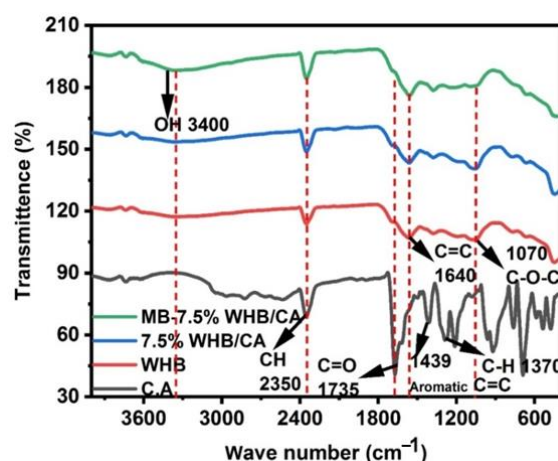
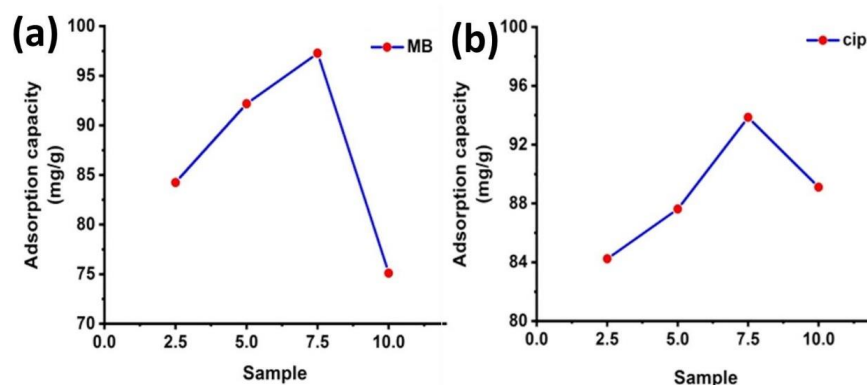


Figure 3. FTIR spectra of WHB, WHB/CA, and MB-WHB/CA.

### 2.4. Adsorption Experiments

Adsorption experiments were carried out by selecting the optimum impregnation ratio of WHB and CA. Mixing 0.1 g of adsorbent with 100 mL of dye solution and 100 mL (100 mg/L) of ciprofloxacin solution at room temperature for 160 minutes at  $25\text{ }^{\circ}\text{C}$  on an orbital shaker at 100 RPM yielded the best impregnation ratio. It was seen from the results

that the modified sample of 7.5% WHB/CA (wheat husk biochar/cinnamic acid) showed maximum adsorption capacity against both adsorbates. Figure 4a shows the plot of impregnation ratios of the samples vs. adsorption capacity of MB, while Figure 4b shows the plot of impregnation ratios of the samples vs. adsorption capacity of Ciprofloxacin. It is inferred from the results that a sample of 7.5% WHB/CA showed the highest adsorption capacity for both adsorbates. So, the whole of the work was performed on a 7.5% WHB/CA sample.



**Figure 4.** Plot of impregnation ratio vs. adsorption capacity of MB (a) and adsorption capacity of ciprofloxacin (b).

#### 2.4.1. Effect of Adsorbent Dosage

The effect of the adsorbent dosage was evaluated by changing the adsorbent dosage from 50 mg to 200 mg in 100 mL of dye solution. The adsorption percentage was enhanced by increasing the dosage of the adsorbent from 83.155 to 99%, after which it became constant, which indicates that 100 mg of adsorbent dosage is sufficient for the maximum removal of pollutants; so, in this work, 100 mg of adsorbent dosage was used in all experiments. This increase in adsorption percentage might be due to an increase in adsorption sites. The adsorbent dose surface area increased, and thus, the adsorption rate also increased. However, further enhancement or poor increment in the adsorption rate was due to the unavailability of MB binding sites (Figure 5a) [48].

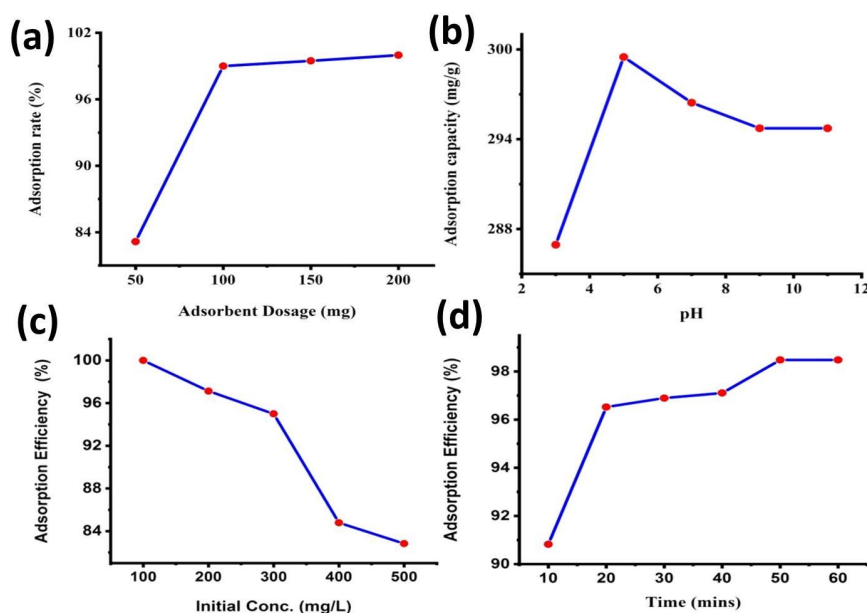


**Figure 5.** Effect of parameters on MB sorption, effect of adsorbent dosage (a), effect of pH (b), effect of initial conc. (c), and effect of contact time (d).

#### 2.4.2. Effect of pH

The pH of wastewater is a very important parameter that may affect the removal rate of the pollutant, so the effect of pH on the adsorption rate was monitored by changing the pH from 3 to 11. The MB removal rate was lowest at pH 3, and the adsorption percentage increased from 95.658% to 99.6% as the pH increased from 3 to 5. So, the maximum removal ratio was obtained at pH 5, which decreased, and then became almost constant. This indicates that sorption is mainly due to hydrogen bonding functional groups ( $-\text{NH}^+$ ,  $\text{SO}^{-3}$ ) in MB and hydroxyl groups present in the adsorbent. For this reason, all experiments were performed at pH 5. Such results were reported by Jasmin S et al. (Figure 5b) [49].

#### 2.4.3. Effect of Initial Concentration of Dye

The effect of the initial dye concentration was studied by adjusting the dye concentration from 100 to 500 mg/L, while keeping the other parameters constant. It was discovered from the data that the sorption rate was initially high, which could be related to the presence of a significant number of active sites on the adsorbent. The sorption rate gradually decreased after fast MB diffusion from the aqueous solution to the adsorbent surface. This could be attributed to the saturation of all active sites on the adsorbent's surface, as well as dye molecules penetrating the adsorbent's pores, lowering the rate of sorption (Figure 5c) [50].

#### 2.4.4. Effect of Contact Time

An adsorption process is mainly affected by contact time. To elucidate the effect of time on the adsorption process, the contact time was varied in the range of 10–60 min at 100 rpm on an orbital shaker, while other parameters were kept constant. The results showed that a maximum adsorption of up to 96.52% was achieved in the early 20 min. Initially, the adsorption rate was very high, which might be due to the presence of enough active sites on the surface of the adsorbent, but as time increased, these sites were gradually filled, clogging the sorption sites, and hence, the adsorption rate slowly increased, and after forty minutes, it became constant. Therefore, the contact time was optimized as 120 min (Figure 5d) [51].

#### 2.4.5. Adsorption Isotherms

Adsorption isotherms are important to the understanding of the mechanism of interaction. The adsorption mechanism of MB on the adsorbent was determined by using the Langmuir and Freundlich models, and their respective parameters are shown in Table 1. It was shown that the  $R^2$  value was 0.97627 and 0.94287 for the Langmuir and Freundlich isotherms, respectively. This showed that adsorption isotherm properties are consistent with the Langmuir isotherm. The Langmuir isotherm is based on a monolayer adsorption mechanism on a homogenous surface. Figure 6a shows the isothermal plot for the Langmuir isotherm, while Figure 6b shows the isotherm plot for the Freundlich isotherm. These two Figures demonstrate that the adsorption mechanism was based on the Langmuir isotherm.

**Table 1.** Parameters of Langmuir and Freundlich isotherm.

Adsorption Model	Isotherm Parameters	$R^2$
Freundlich Model	$K_f = 111.9026 \text{ mg/g}$ $1/n = 3.34314$	0.94287
Langmuir Model	$Q_{\max} = 427.35 \text{ mg/g}$ $K_L = 27721.8 \text{ m}^{-1} \cdot \text{g}^{-1}$ $R_L = 0.003314$	0.97627

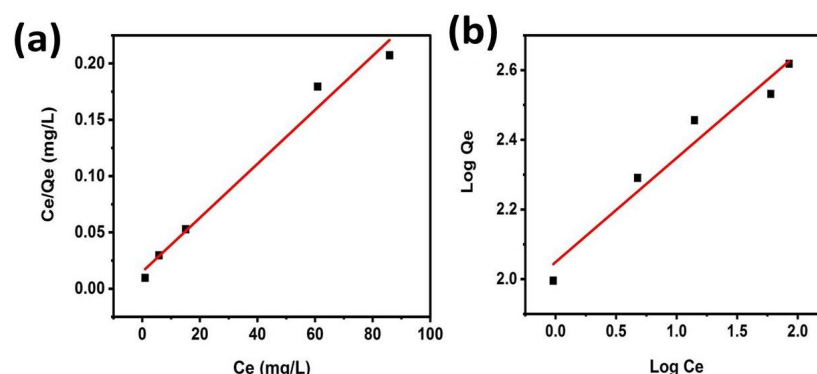


**Figure 6.** Langmuir graph (a) and Freundlich graph (b) MB adsorption on WHB/CA at pH = 5, 0.1 g biochar, T = 25 °C, and initial concentration of 300 mg/L.

#### 2.4.6. Adsorption Kinetics

Adsorption kinetics is very important for the investigation of adsorption efficiency and the adsorption mechanism. So, kinetic parameters were evaluated by using two models, i.e., pseudo-first-order kinetics and pseudo-second-order kinetics. Their parameters are shown in Table 2, and their plots are shown in Figure 7a,b. The correlation coefficients ( $R^2$ ) for pseudo-second-order and pseudo-first-order were ( $R^2$ ) 0.9999 and 0.83843, respectively, and the adsorption capacity from pseudo-second-order was consistent with the experimental value.

**Table 2.** Parameters of pseudo-first- and pseudo-second-order.

Pseudo-First-Order Model	$C_0$ (mg/L)	$Q_e$ (mg/g) (exp)	$Q_e$ (mg/g) (cal)	$K_1$ (min <sup>-1</sup> )	$R^2$
	300	299.495	2162.46	−0.0005745	0.8383
Pseudo-Second-Order Model	$C_0$ (mg/L)	$Q_e$ (mg/g) (exp)	$Q_e$ (mg/g) (cal)	$K_2$ (g.mg <sup>-1</sup> min <sup>-1</sup> )	$R^2$
	200	299.495	300.300	321.54	0.9999

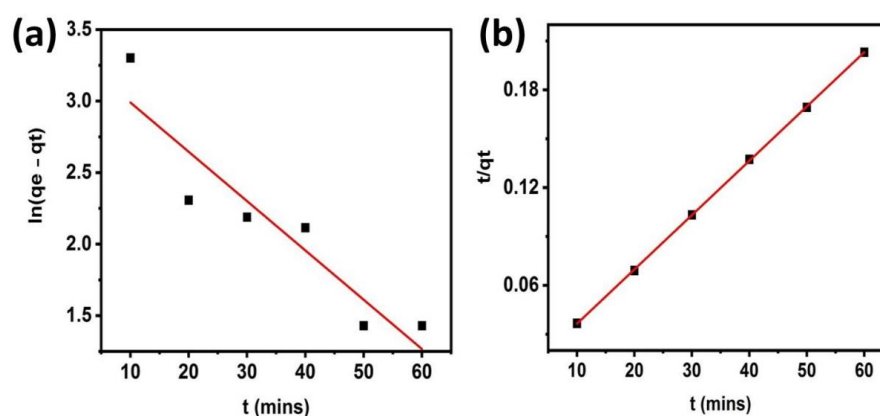


**Figure 7.** Plot of pseudo-first-order (a) and plot of pseudo-second-order (b).

#### 2.5. Investigation of Adsorption Mechanism Based on DFT Analysis

To explore molecular communications among adapted biochar and MB, batch adsorption experiments were combined with density functional theory (DFT). Modified wheat husk biochar has a much-enhanced ability to adsorb MB and CIP. To investigate the adsorption mechanism and possible sites of adsorption, a DFT study was performed by using the 6–31G Hartree–Fock method. The structures of the adsorbates and adsorbents were optimized, and their molecular electrostatic potentials (MEP) were calculated. The MEP analysis showed the region of upper and lower potential, as designated by blue and red colors, respectively.

Figure 8a shows the MEP diagram of cellulose cinnamate, representing possible sites of attack. The hydrogen of the hydroxyl group is shown in blue color, having maximum potential. Hence, it was a possible site of attack by the nucleophile. While the red color indicates that the oxygen of the carbonyl group had the least potential, it was a possible site of attack for an electrophile. While the MEP of MB is shown in Figure 8b, the phenothiazine nitrogen atom was at a lower potential, represented by red, and could be a target for an electrophilic attack, whereas the atoms of dimethylamine benzene were at a higher potential, represented by blue, and could be a target for a nucleophilic assault. As a result of the MEP analysis, electrophilic interaction in the nitrogen of methylene blue and nucleophilic interaction in the dimethylamine group were discovered. The MEP diagram of CIP in neutral form is shown in Figure 8c. It shows that oxygen attached to the benzene ring and oxygen of the carbonyl group showed the least potential. Hence, these were the possible sites for the attack of the electrophile, while hydrogen of the carbonyl group showed maximum potential, so it was a possible site for the attack of the nucleophile. MEP of CIP in zwitterion form is shown in Figure 8d; here, the oxygen of the carbonyl group and oxygen-bearing negative charge showed the least potential, so these were the possible sites for the attack of the electrophile, while the nitrogen of the amino group showed maximum potential, and hence, it was a possible site for the attack of the nucleophile. In this way, MB and CIP were adsorbed on the surface of WHB/CA and effectively improved the quality of wastewater. [52].

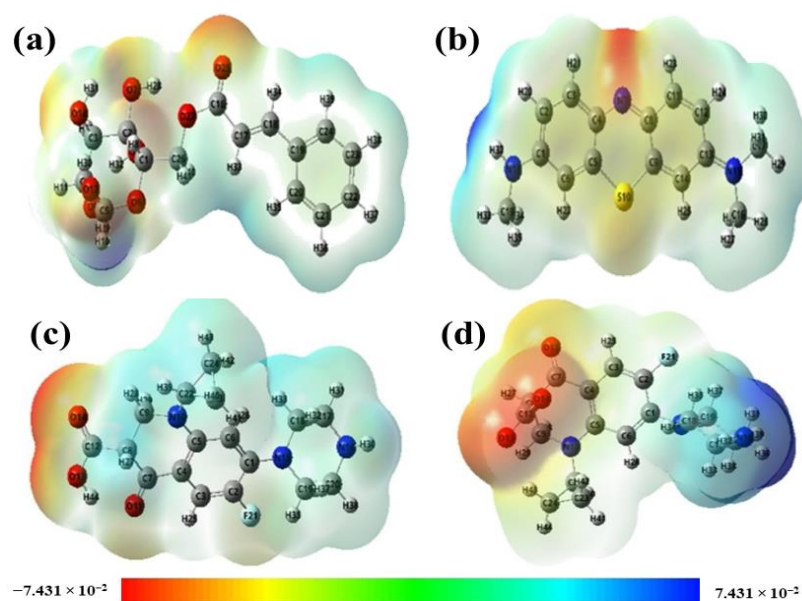


**Figure 8.** MEP of cellulose cinnamate (a), MEP of MB (b), MEP of CIP in neutral form (c), and MEP diagram of CIP in zwitterion form (d).

#### 2.5.1. Possible Interactions of CIP with Modified Biochar

pH plays an important role during the adsorption of ciprofloxacin, as CIP exists in protonated, deprotonated, neutral, and zwitterion forms at different pH. Hence, the mechanism of adsorption of ciprofloxacin is highly dependent on the pH. So, pH is a crucial parameter for the adsorption of ciprofloxacin on modified biochar. CIP exists in protonated form at  $\text{pH} < 6.09$  and deprotonated at  $\text{pH} > 8.64$ , while it exists in neutral and zwitterion form at  $6.09 < \text{pH} < 8.64$ , but here, the zwitterion form is more dominated than the neutral form. At  $\text{pH} < 6.09$ , the amine group of ciprofloxacin gets protonated; hence, the protonated form exists at this pH, while at  $\text{pH} > 8.64$ , the amine group of CIP gets deprotonated, so at this pH, the deprotonated form exists. During the  $6.09 < \text{pH} < 8.64$ , the amine group of CIP gets protonated, and the carboxyl group is deprotonated. So, at this pH, both positive and negative charges exist in CIP. Hence, at this pH, CIP exists in form zwitterion. All forms

of CIP have a great attraction to modified biochar. This attraction is based on H-bonding, pi-pi interaction, pore diffusion, and EDA (electron donor-acceptor) interaction. CIP has electronegative and electropositive functional groups that form a hydrogen bond with modified biochar. In zwitterion form, CIP has positively charged  $\text{NH}^+$  and negatively charged  $\text{C}-\text{O}^-$ ; both of these make a hydrogen bond with modified biochar. Moreover, the presence of a highly electronegative fluorine atom also provides an extra site for electron acceptance from modified biochar. Hence, EDA interaction also plays a part during the adsorption of CIP on WHB/CA. Figure 9 shows various forms of CIP at different pH, while Figures 2 and 3 show the interaction of modified biochar with the neutral form of CIP and with the zwitterion form of CIP [53].

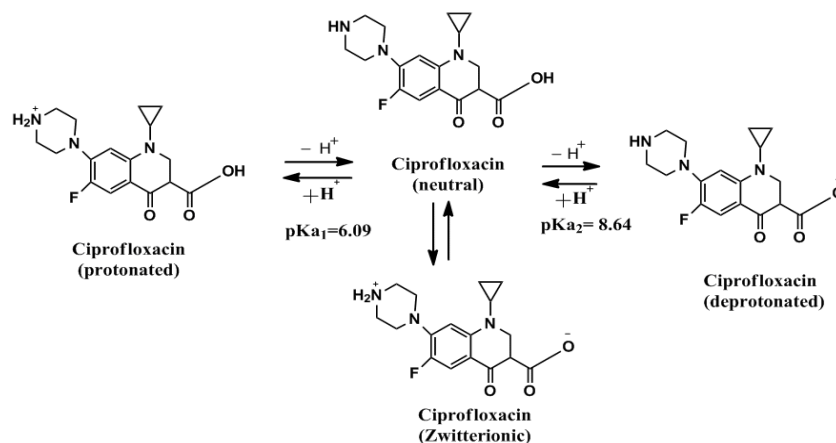


**Figure 9.** Forms of ciprofloxacin at different pH.

### 2.5.2. Interaction Mechanism Based upon HOMO and LUMO

The interaction mechanism was explored by calculating the HOMO and LUMO of ciprofloxacin in neutral form and zwitterion form (Figure 10). The calculated energy gap between HOMO and LUMO of CIP in neutral form was 0.12974, while for zwitterion form, it was 0.04452, which showed that more energy is required for the transition from LUMO to HOMO for CIP in neutral form, while less energy is required for the transition in the case of CIP in zwitterion form, suggesting that it is more reactive than neutral form. A possible reaction mechanism for both neutral and zwitterion forms is given in Figures 11 and 12, respectively, and their parameters are shown in Table 3 [54]. The WHB/CA for the adsorption of MB and CIP was compared with other adsorbents in terms of the maximum uptake of different adsorbents, as reported in Table 4.

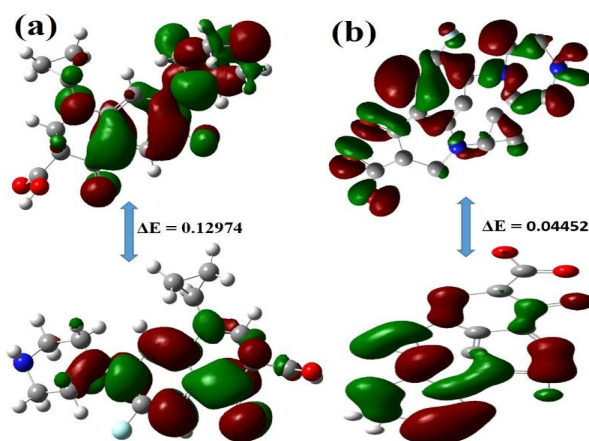


**Figure 10.** Interaction mechanism of CIP in neutral form (a) and zwitterion form (b) with modified biochar based on HOMO and LUMO.

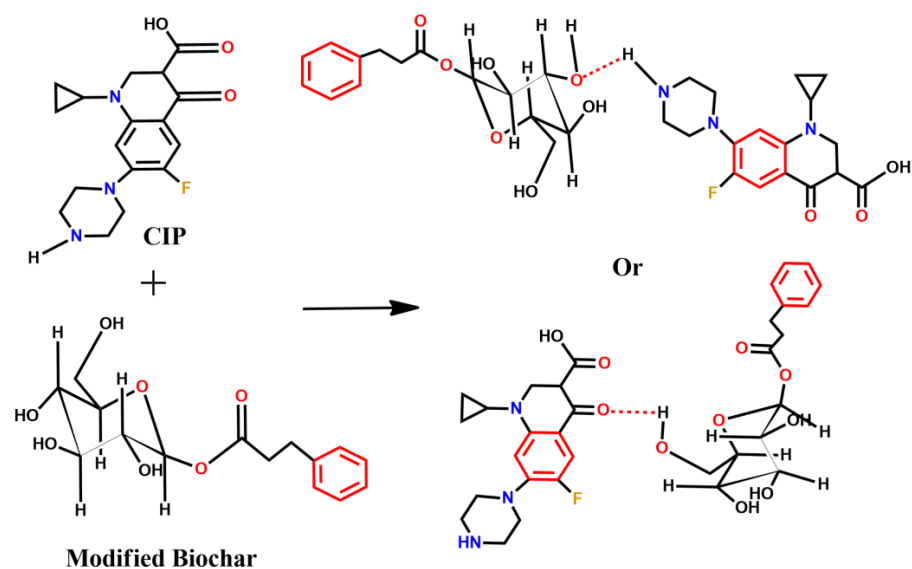


Figure 11. Interaction of CIP in neutral form with modified biochar.

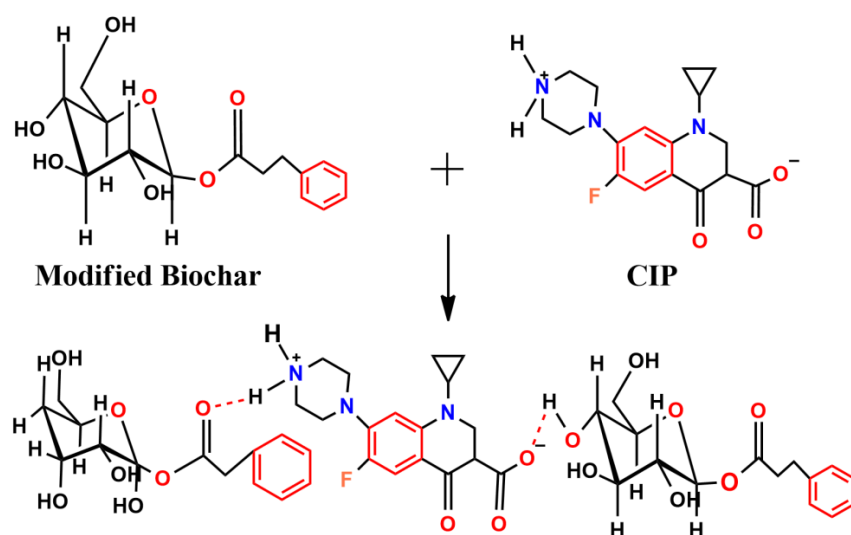


Figure 12. Interaction mechanism of CIP in zwitterion form with modified biochar.

Table 3. HOMO and LUMO energy values and other parameters.

Parameters (eV)	CIP (Neutral)	CIP (Zwitterion)
$E_{\text{LUMO}}$	−0.21903	−0.10424
$E_{\text{HOMO}}$	−0.08929	−0.05972
Energy gap ( $E_{\text{HOMO}}-E_{\text{LUMO}}$ )	0.12974	0.04452
Ionization potential ( $I = -E_{\text{HOMO}}$ )	0.08929	0.05972
Electron affinity ( $A = -E_{\text{LUMO}}$ )	0.21903	0.10424
Chemical hardness ( $\eta = (I-A)/2$ )	−0.06487	−0.02226
Chemical softness ( $\zeta = 1/2\eta$ )	−7.7077	−1.34141
Electronegativity ( $\chi = (I + A)/2$ )	0.15416	0.08198
Chemical potential ( $\mu = -(I + A)/2$ )	−0.15416	−0.08198
Electrophilicity index ( $\omega = \mu^2/2\eta$ )	−0.183135	−0.15094

**Table 4.** Comparison of maximum adsorption capacities of biochar prepared from different sources.

S. N.	Adsorbent	Adsorption Capacity (mg/g)	Reference
1	Wheat bran sawdust/Fe <sub>3</sub> O <sub>4</sub> composite	51.28	[55]
2	Biochar from mixed municipal discarded material (MMDM)	7.2	[56]
3	Wodyetia bifurcate biochar	149.3	[57]
4	Mangolia Gradiflora Linn Leaf biochar (MGB)	101.27	[58]
5	Sour lemon saw dust	52.4	[59]
6	Date palm sawdust	54	[59]
7	Eucalyptus sawdust	53.5	[59]
8	Reed	53.23	[60]
9	Ficus Carica Bast Activated carbon	47.62	[61]
10	Biowaste sawdust	58.14	[62]
11	Peanut shell biochar	208	[49]
13	WHB/CA	427.35	This study

### 3. Materials and Methods

The wheat husk used in this work was collected from the Alnoor flour mill in Pasrur, Punjab, Pakistan. All reagents, including sodium hydroxide, nitric acid, cinnamic acid, hydrochloric acid, and methylene blue, were acquired from Sigma Aldrich and used as received. Throughout the experiment, distilled water was used. The stock solutions of methylene blue (500 mg/L) and ciprofloxacin (500 mg/L) were prepared in distilled water, while other required solutions were prepared by making dilutions from stock solutions. In this experiment, pH and temperature were measured using a digital meter. Concentrations of MB and ciprofloxacin were determined at 698 nm and 276 nm, respectively, via a UV-Visible spectrophotometer.

#### 3.1. Preparation of Biochar

Firstly, the washing of wheat husk (WH) was performed with tap water and then with distilled water several times to remove surface impurities. The washed WH was dried for 24 h at 353 K and then chilled to room temperature before being crushed [63]. WH was transformed into biochar by slow pyrolysis in an electrical furnace at a heating rate of 10 °C/min and held for 2 h at 800 °C. Biochar was obtained under a limited supply of oxygen [64,65]. It was then crushed with a pestle and mortar to generate a fine powder, which was sieved to produce particles with a particle size of 40–60 mesh and stored in a glass bottle with the words “Wheat Husk Biochar” on it (WHB).

#### 3.2. Modification of WHB

The modification of WHB was performed by the method reported by Gong et al., with slight modifications [66]. WHB was modified with cinnamic acid (C.A) at different impregnation ratios of 2.5%, 5%, 7.5%, and 10% (WHB/CA, W/W), followed by magnetic stirring for 2 h at room temperature. Esterification was achieved by adding 2–3 drops of nitric acid. It was then dried in a drying oven at 100 °C for 24 h, before being stored in a glass bottle. The optimum impregnation ratio was determined by dissolving 100 mg of adsorbent in 100 mL of dye solution at room temperature and shaking it for 160 min at 25 °C on an orbital shaker at 100 RPM. It was seen from the results that a modified sample of 7.5% WHB/CA (wheat husk biochar/cinnamic acid) showed maximum adsorption. So, the whole of the work was performed on this sample and named 7.5% WHB/CA.

#### 3.3. Characterization

To investigate the surface topology and elemental content of the sample, scanning electron microscopy (SEM), equipped with energy dispersive spectroscopy (EDS) (FEI Nova 450 Nano SEM), was performed. Functional groups present in the samples were analyzed by using Fourier transform infrared spectroscopy (IRSpirit-T, Shimadzu). For

this, FTIR spectra of all impregnation ratios, WHB, and samples after adsorbing MB (TWH) were recorded and analyzed. The concentration of pollutants was determined via a UV-Vis spectrophotometer (Cecil 7400S). The crystallinity and phase of the adsorbent were evaluated by X-ray diffraction (XRD) measurements in the range of 10–80° (2θ).

### 3.4. Batch Adsorption Study

The experiments were performed in batch mode in a 100 mL Erlenmeyer flask, shaken in an orbital shaker (orbital shaker incubator ES 20) at 120 rpm for 120 min. NaOH and HCl were used to adjust the initial pH. The effect of various parameters was investigated by performing adsorption of MB at various initial concentrations (100–500 mg/L), adsorbent dosages (0.5 g–0.2 g), times (10–60 min), and pH from 3–11. For reproducibility and accuracy, each experiment was repeated thrice. The concentrations of dye and ciprofloxacin were determined using a Cecil 7400S UV-Vis spectrophotometer at the wavelength of maximum absorbance,  $\lambda_{\max} = 664$  nm and 278 nm, respectively. Adsorption ability  $q_e$  (mg/g) and removal efficiency (%) were computed using Equations (1) and (2), respectively.

$$q_e = \frac{(C_0 - C_t)V}{W} \quad (1)$$

$$\% = \frac{C_0 - C_e}{C_0} \quad (2)$$

Here,  $C_e$  and  $C_0$  represent the initial and equilibrium concentrations (mg/g) of the adsorbate, while  $V$  represents the volume of the solution (L), and  $W$  represents the weight of the adsorbent (g) used.

### 3.5. Adsorption Isotherm

Adsorption isotherms depict the relationship between adsorbents and adsorbates. They depict the relationship between the amount of adsorbate adsorbed on the adsorbent and amount present in the solution at equilibrium. The adsorption mechanism can also be inferred from these models. In this work, two adsorption isothermal models were employed to analyze adsorption equilibrium data, i.e., the Freundlich and Langmuir models. The Langmuir model is based on the monolayer adsorption mechanism on the homogenous surface of the adsorbent [52]. The Langmuir isotherm can be given by the following equation.

$$\frac{C_e}{Q_e} = \frac{1}{K_L q_m} + \frac{1}{q_m} C_e \quad (3)$$

Here,  $C_e$  represents the equilibrium concentration (mg/L), and  $Q_e$  represents the equilibrium adsorption capacity (mg/g), while  $q_m$  is the maximum adsorption capacity calculated by the Langmuir isotherm, and  $K_L$  is the Langmuir constant. Table 1 shows that the data obtained by the Langmuir isotherm,  $q_e$ ,  $K_L$ , and  $q_m$  are computed by the slope and intercept of the fitted line of the Langmuir isotherm.

The Freundlich isotherm relies on the assumption that adsorption occurs on the heterogeneous surface through a multi-layer adsorption mechanism [49]. The Freundlich isotherm is given by the following equation.

$$\ln q_e = \frac{1}{n} \ln C_e + \ln K_F \quad (4)$$

$K_F$  is the Freundlich constant (L/mg),  $n$  is a constant number that is related to adsorption strength, and  $1/n$  shows adsorption favorability, which is related to the degree of heterogeneity of the surface [67].

### 3.6. Adsorption Kinetics

To explain adsorption characteristics and the adsorption mechanism, kinetic models were studied. For the adsorption process, two commonly used models were employed:

pseudo-first-order and pseudo-second-order. At various time intervals, the concentration of the solution was determined, and the adsorption capacity at that time is defined as  $q_t$ , calculated by the following equation.

Pseudo-first-order is given by Equation (5).

$$\ln\left(\frac{q_e}{q_e - q_t}\right) = \frac{K_1 t}{2.303} \quad (5)$$

$K_1$  (1/min) shows the adsorption rate constant for pseudo-first-order, while  $q_t$  and  $q_e$  show adsorption capacities at time  $t$  and equilibrium, respectively.

A pseudo-second-order kinetic model is given by Equation (6).

$$\frac{t}{q_t} = \frac{t}{q_e} + \frac{1}{K_2 q_e^2} \quad (6)$$

$q_t$  (mg/g) and  $q_e$  (mg/g) are the adsorption capacities at time  $t$  and equilibrium, respectively, and  $K_2$  is a pseudo-second-order constant.

#### 4. Conclusions

The WH-based adsorbent was prepared through acid modification. Optimal conditions were pH 5, a dosage of 0.1 g, an initial dye concentration of 300 mg/L, and a contact time of 2 h. Results showed that the maximum adsorption capacity was 299.493 mg/g for MB and 94.03% for CIP. The best fit for the adsorption process was pseudo-second-order kinetics combined with the Langmuir isotherm. Hence, their values also proved that WHB/CA is the most acceptable adsorbent material for the removal of MB from wastewater. This study also showed that WHB/CA is an efficient, novel, and cost-effective adsorbent for wastewater treatment. Its synthesis also provides a new way for the utilization of wheat husk.

**Author Contributions:** U.H.: writing—original draft. S.M.: supervision, funding acquisition, and writing—review and editing. M.A.K.: writing—editing, conceptualization, software, and resources. M.S.R., K.S.M., and M.H.: editing and reviewing. All authors have read and agreed to the published version of the manuscript.

**Funding:** This research was funded by the Higher Education Commission (HEC) in Pakistan (NRPU-Project No. 16132). Taif University Researchers Supporting Project number (TURSP-2020/01), Taif University, Taif, Saudi Arabia.

**Data Availability Statement:** Not applicable.

**Acknowledgments:** The authors are thankful to IRCBM, Comsats University Islamabad Lahore campus, and the University of Mianwali for providing characterization facilities. Taif University Researchers Supporting Project number (TURSP-2020/01), Taif University, Taif, Saudi Arabia.

**Conflicts of Interest:** The authors declare no conflict of interest.

**Sample Availability:** Not available.

#### References

1. Hokkanen, S.; Bhatnagar, A.; Sillanpää, M. A review on modification methods to cellulose-based adsorbents to improve adsorption capacity. *Water Res.* **2016**, *91*, 156–173. [\[CrossRef\]](#)
2. Lu, F.; Astruc, D. Nanocatalysts and other nanomaterials for water remediation from organic pollutants. *Coord. Chem. Rev.* **2020**, *408*, 213180. [\[CrossRef\]](#)
3. Li, G.; Li, J.; Tan, W.; Yang, M.; Wang, H.; Wang, X. Effectiveness and mechanisms of the adsorption of carbendazim from wastewater onto commercial activated carbon. *Chemosphere* **2022**, *304*, 135231. [\[CrossRef\]](#)
4. Lan, T.; Cao, F.; Cao, L.; Wang, T.; Yu, C.; Wang, F. A comparative study on the adsorption behavior and mechanism of pesticides on agricultural film microplastics and straw degradation products. *Chemosphere* **2022**, *303*, 135058. [\[CrossRef\]](#) [\[PubMed\]](#)
5. Mohanraj, J.; Durgalakshmi, D.; Balakumar, S.; Aruna, P.; Ganesan, S.; Rajendran, S.; Naushad, M. Low cost and quick time absorption of organic dye pollutants under ambient condition using partially exfoliated graphite. *J. Water Process Eng.* **2020**, *34*, 101078. [\[CrossRef\]](#)
6. Sen, T.K.; Afroze, S.; Ang, H.M. Equilibrium, Kinetics and Mechanism of Removal of Methylene Blue from Aqueous Solution by Adsorption onto Pine Cone Biomass of *Pinus radiata*. *Water Air Soil Pollut.* **2011**, *218*, 499–515. [\[CrossRef\]](#)

7. Kafshgari, L.A.; Ghorbani, M.; Azizi, A. Fabrication and investigation of  $\text{MnFe}_2\text{O}_4/\text{MWCNTs}$  nanocomposite by hydrothermal technique and adsorption of cationic and anionic dyes. *Appl. Surf. Sci.* **2017**, *419*, 70–83. [\[CrossRef\]](#)
8. Ghosh, D.; Bhattacharyya, K.G. Adsorption of methylene blue on kaolinite. *Appl. Clay Sci.* **2002**, *20*, 295–300. [\[CrossRef\]](#)
9. Senthilkumaar, S.; Varadarajan, P.; Porkodi, K.; Subbhuraam, C. Adsorption of methylene blue onto jute fiber carbon: Kinetics and equilibrium studies. *J. Colloid Interface Sci.* **2005**, *284*, 78–82. [\[CrossRef\]](#)
10. Durrani, W.Z.; Nasrullah, A.; Khan, A.S.; Fagieh, T.M.; Bakhsh, E.M.; Akhtar, K.; Khan, S.B.; Din, I.U.; Khan, M.A.; Bokhari, A. Adsorption efficiency of date palm based activated carbon-alginate membrane for methylene blue. *Chemosphere* **2022**, *302*, 134793. [\[CrossRef\]](#)
11. Adefurin, A.; Sammons, H.; Jacqz-Aigrain, E.; Choonara, I. Ciprofloxacin safety in paediatrics: A systematic review. *Arch. Dis. Child.* **2011**, *96*, 874–880. [\[CrossRef\]](#)
12. Ashfaq, M.; Li, Y.; Rehman, M.S.U.; Zubair, M.; Mustafa, G.; Nazar, M.F.; Yu, C.-P.; Sun, Q. Occurrence, spatial variation and risk assessment of pharmaceuticals and personal care products in urban wastewater, canal surface water, and their sediments: A case study of Lahore, Pakistan. *Sci. Total Environ.* **2019**, *688*, 653–663. [\[CrossRef\]](#) [\[PubMed\]](#)
13. Arsand, J.B.; Hoff, R.B.; Jank, L.; Bussamara, R.; Dallegrave, A.; Bento, F.M.; Kmetzsch, L.; Falcão, D.A.; Peralba, M.D.C.R.; Gomes, A.D.A.; et al. Presence of antibiotic resistance genes and its association with antibiotic occurrence in Dilúvio River in southern Brazil. *Sci. Total Environ.* **2020**, *738*, 139781. [\[CrossRef\]](#) [\[PubMed\]](#)
14. Falyouna, O.; Maamoun, I.; Bensaida, K.; Tahara, A.; Sugihara, Y.; Eljamal, O. Encapsulation of iron nanoparticles with magnesium hydroxide shell for remarkable removal of ciprofloxacin from contaminated water. *J. Colloid Interface Sci.* **2022**, *605*, 813–827. [\[CrossRef\]](#) [\[PubMed\]](#)
15. Jafari, K.; Heidari, M.; Rahmanian, O. Wastewater treatment for Amoxicillin removal using magnetic adsorbent synthesized by ultrasound process. *Ultrason. Sonochemistry* **2018**, *45*, 248–256. [\[CrossRef\]](#)
16. Arian, O.A. Degradation and metabolization of chlortetracycline during the anaerobic digestion of manure from medicated calves. *J. Hazard. Mater.* **2008**, *158*, 485–490. [\[CrossRef\]](#)
17. Sturini, M.; Speltini, A.; Maraschi, F.; Rivagli, E.; Pretali, L.; Malavasi, L.; Profumo, A.; Fasani, E.; Albini, A. Sunlight photodegradation of marbofloxacin and enrofloxacin adsorbed on clay minerals. *J. Photochem. Photobiol. A Chem.* **2015**, *299*, 103–109. [\[CrossRef\]](#)
18. Gomes, J.; Costa, R.; Quinta-Ferreira, R.M.; Martins, R.C. Application of ozonation for pharmaceuticals and personal care products removal from water. *Sci. Total Environ.* **2017**, *586*, 265–283. [\[CrossRef\]](#)
19. Hirose, J.; Kondo, F.; Nakano, T.; Kobayashi, T.; Hiro, N.; Ando, Y.; Takenaka, H.; Sano, K. Inactivation of antineoplastics in clinical wastewater by electrolysis. *Chemosphere* **2005**, *60*, 1018–1024. [\[CrossRef\]](#)
20. Zhang, X.; Guo, W.; Ngo, H.H.; Wen, H.; Li, N.; Wu, W. Performance evaluation of powdered activated carbon for removing 28 types of antibiotics from water. *J. Environ. Manag.* **2016**, *172*, 193–200. [\[CrossRef\]](#)
21. Wang, J.; Wang, S. Removal of pharmaceuticals and personal care products (PPCPs) from wastewater: A review. *J. Environ. Manag.* **2016**, *182*, 620–640. [\[CrossRef\]](#) [\[PubMed\]](#)
22. Košutić, K.; Dolar, D.; Ašperger, D.; Kunst, B. Removal of antibiotics from a model wastewater by RO/NF membranes. *Sep. Purif. Technol.* **2007**, *53*, 244–249. [\[CrossRef\]](#)
23. Doğan, E.C. Investigation of ciprofloxacin removal from aqueous solution by nanofiltration process. *Glob. Nest J.* **2016**, *18*, 291–308.
24. Sun, S.P.; Hatton, T.A.; Chung, T.-S. Hyperbranched Polyethyleneimine Induced Cross-Linking of Polyamide-imide Nanofiltration Hollow Fiber Membranes for Effective Removal of Ciprofloxacin. *Environ. Sci. Technol.* **2011**, *45*, 4003–4009. [\[CrossRef\]](#)
25. Ahmadi, S.; Osagie, C.; Rahdar, S.; Khan, N.A.; Ahmed, S.; Hajini, H. Efficacy of persulfate-based advanced oxidation process (US/PS/Fe<sub>3</sub>O<sub>4</sub>) for ciprofloxacin removal from aqueous solutions. *Appl. Water Sci.* **2020**, *10*, 187. [\[CrossRef\]](#)
26. Mondal, S.K.; Saha, A.K.; Sinha, A. Removal of ciprofloxacin using modified advanced oxidation processes: Kinetics, pathways and process optimization. *J. Clean. Prod.* **2018**, *171*, 1203–1214. [\[CrossRef\]](#)
27. Barisci, S.; Turkey, O. Applications of response surface methodology (RSM) for the optimization of ciprofloxacin removal by electrocoagulation. In Proceedings of the IWA Balkan Young Water Professionals Conference, Thessaloniki, Greece, 10–12 May 2015; pp. 10–12.
28. Gupta, V.K.; Jain, R.; Varshney, S. Removal of Reactofix golden yellow 3 RFN from aqueous solution using wheat husk—An agricultural waste. *J. Hazard. Mater.* **2007**, *142*, 443–448. [\[CrossRef\]](#)
29. Ji, L.; Chen, W.; Duan, L.; Zhu, D. Mechanisms for strong adsorption of tetracycline to carbon nanotubes: A comparative study using activated carbon and graphite as adsorbents. *Environ. Sci. Technol.* **2009**, *43*, 2322–2327. [\[CrossRef\]](#)
30. Alnajrani, M.N.; Alsager, O.A. Removal of antibiotics from water by polymer of intrinsic microporosity: Isotherms, kinetics, thermodynamics, and adsorption mechanism. *Sci. Rep.* **2020**, *10*, 794. [\[CrossRef\]](#)
31. Aarab, N.; Hsini, A.; Esseki, A.; Laabd, M.; Lakhmiri, R.; Albourine, A. Removal of an emerging pharmaceutical pollutant (metronidazole) using PPY-PANi copolymer: Kinetics, equilibrium and DFT identification of adsorption mechanism. *Groundw. Sustain. Dev.* **2020**, *11*, 100416. [\[CrossRef\]](#)
32. Kong, Y.; Wang, L.; Ge, Y.; Su, H.; Li, Z. Lignin xanthate resin-bentonite clay composite as a highly effective and low-cost adsorbent for the removal of doxycycline hydrochloride antibiotic and mercury ions in water. *J. Hazard. Mater.* **2019**, *368*, 33–41. [\[CrossRef\]](#) [\[PubMed\]](#)

33. Kalhori, E.M.; Al-Musawi, T.; Ghahramani, E.; Kazemian, H.; Zarrabi, M. Enhancement of the adsorption capacity of the light-weight expanded clay aggregate surface for the metronidazole antibiotic by coating with MgO nanoparticles: Studies on the kinetic, isotherm, and effects of environmental parameters. *Chemosphere* **2017**, *175*, 8–20. [\[CrossRef\]](#)
34. Alshorifi, F.T.; Ali, S.L.; Salama, R.S. Promotional Synergistic Effect of Cs–Au NPs on the Performance of Cs–Au/MgFe<sub>2</sub>O<sub>4</sub> Catalysts in Catalysis 3,4-Dihydropyrimidin-2(1H)-Ones and Degradation of RhB Dye. *J. Inorg. Organomet. Polym. Mater.* **2022**, 1–12. [\[CrossRef\]](#)
35. Bakry, A.M.; Alamier, W.M.; Salama, R.S.; El-Shall, M.S.; Awad, F.S. Remediation of water containing phosphate using ceria nanoparticles decorated partially reduced graphene oxide (CeO<sub>2</sub>-PRGO) composite. *Surfaces Interfaces* **2022**, *31*, 102006. [\[CrossRef\]](#)
36. Ibrahim, A.A.; Salama, R.S.; El-Hakam, S.A.; Khder, A.S.; Ahmed, A.I. Synthesis of 12-tungstophosphoric acid supported on Zr/MCM-41 composite with excellent heterogeneous catalyst and promising adsorbent of methylene blue. *Colloids Surf. A Physicochem. Eng. Asp.* **2021**, *631*, 127753. [\[CrossRef\]](#)
37. Chen, W.-R.; Huang, C.-H. Adsorption and transformation of tetracycline antibiotics with aluminum oxide. *Chemosphere* **2010**, *79*, 779–785. [\[CrossRef\]](#)
38. Garg, V.K.; Amita, M.; Kumar, R.; Gupta, R.J.D. Basic dye (methylene blue) removal from simulated wastewater by adsorption using indian rosewood sawdust: A timber industry waste. *Dye. Pigment.* **2004**, *63*, 243–250. [\[CrossRef\]](#)
39. Ngah, W.W.; Hanafiah, M.M. Removal of heavy metal ions from wastewater by chemically modified plant wastes as adsorbents: A review. *Bioresour. Technol.* **2008**, *99*, 3935–3948. [\[CrossRef\]](#)
40. Khan, T.S.; Mubeen, U. Wheat straw: A pragmatic overview. *Curr. Res. J. Biol. Sci* **2012**, *4*, 673–675.
41. Li, G.; Zhu, W.; Zhang, C.; Zhang, S.; Liu, L.; Zhu, L.; Zhao, W. Effect of a magnetic field on the adsorptive removal of methylene blue onto wheat straw biochar. *Bioresour. Technol.* **2016**, *206*, 16–22. [\[CrossRef\]](#)
42. Oei, B.C.; Ibrahim, S.; Wang, S.; Ang, H.M.J.B.t. Surfactant modified barley straw for removal of acid and reactive dyes from aqueous solution. *Bioresour. Technol.* **2009**, *100*, 4292–4295. [\[CrossRef\]](#) [\[PubMed\]](#)
43. You, H.; Chen, J.; Yang, C.; Xu, L.J.C.; Physicochemical, S.A.; Aspects, E. Selective removal of cationic dye from aqueous solution by low-cost adsorbent using phytic acid modified wheat straw. *Colloids Surf. A Physicochem. Eng. Asp.* **2016**, *509*, 91–98. [\[CrossRef\]](#)
44. Kuang, Y.; Zhang, X.; Zhou, S. Adsorption of methylene blue in water onto activated carbon by surfactant modification. *Water* **2020**, *12*, 587. [\[CrossRef\]](#)
45. Irfan, M.; Asghar, U.; Nadeem, M.; Nelofer, R.; Syed, Q.; Shakir, H.A.; Qazi, J.I. Statistical optimization of saccharification of alkali pretreated wheat straw for bioethanol production. *Waste Biomass Valorization* **2016**, *7*, 1389–1396. [\[CrossRef\]](#)
46. Lin, Q.; Wang, K.; Gao, M.; Bai, Y.; Chen, L.; Ma, H. Effectively removal of cationic and anionic dyes by ph-sensitive amphoteric adsorbent derived from agricultural waste-wheat straw. *J. Taiwan Inst. Chem. Eng.* **2017**, *76*, 65–72. [\[CrossRef\]](#)
47. Avni, E.; Coughlin, R.W.; Solomon, P.R.; King, H.H. Mathematical modelling of lignin pyrolysis. *Fuel* **1985**, *64*, 1495–1501. [\[CrossRef\]](#)
48. Shah, J.; Jan, M.R.; Jamil, S.; Haq, A.U. Magnetic particles precipitated onto wheat husk for removal of methyl blue from aqueous solution. *Environ. Toxicol. Chem.* **2014**, *96*, 218–226. [\[CrossRef\]](#)
49. Han, X.; Chu, L.; Liu, S.; Chen, T.; Ding, C.; Yan, J.; Cui, L.; Quan, G. Removal of methylene blue from aqueous solution using porous biochar obtained by koh activation of peanut shell biochar. *BioResources* **2015**, *10*, 2836–2849. [\[CrossRef\]](#)
50. Zhu, Y.; Yi, B.; Yuan, Q.; Wu, Y.; Wang, M.; Yan, S. Removal of methylene blue from aqueous solution by cattle manure-derived low temperature biochar. *RSC advances* **2018**, *8*, 19917–19929. [\[CrossRef\]](#)
51. Liang, L.; Xi, F.; Tan, W.; Meng, X.; Hu, B.; Wang, X. Review of organic and inorganic pollutants removal by biochar and biochar-based composites. *Biochar* **2021**, *3*, 255–281. [\[CrossRef\]](#)
52. Guediri, A.; Bouguettoucha, A.; Chebli, D.; Chafai, N.; Amrane, A. Molecular dynamic simulation and DFT computational studies on the adsorption performances of methylene blue in aqueous solutions by orange peel-modified phosphoric acid. *J. Mol. Struct.* **2020**, *1202*, 127290. [\[CrossRef\]](#)
53. Patel, M.; Kumar, R.; Pittman, C.U., Jr.; Mohan, D. Ciprofloxacin and acetaminophen sorption onto banana peel biochars: Environmental and process parameter influences. *Environ. Res.* **2021**, *201*, 111218. [\[CrossRef\]](#) [\[PubMed\]](#)
54. Carabineiro, S.; Thavorn-Amornsri, T.; Pereira, M.; Serp, P.; Figueiredo, J. Comparison between activated carbon, carbon xerogel and carbon nanotubes for the adsorption of the antibiotic ciprofloxacin. *Catal. Today* **2012**, *186*, 29–34. [\[CrossRef\]](#)
55. Pooladi, H.; Foroutan, R.; Esmaeili, H. Synthesis of wheat bran sawdust/Fe<sub>3</sub>O<sub>4</sub> composite for the removal of methylene blue and methyl violet. *Environ. Monit. Assess.* **2021**, *193*, 276. [\[CrossRef\]](#) [\[PubMed\]](#)
56. Hoslett, J.; Ghazal, H.; Mohamad, N.; Jouhara, H. Removal of methylene blue from aqueous solutions by biochar prepared from the pyrolysis of mixed municipal discarded material. *Sci. Total Environ.* **2020**, *714*, 136832. [\[CrossRef\]](#)
57. Dos Santos, K.J.L.; dos Santos, G.E.D.S.; de Sá, Í.M.G.L.; Ide, A.H.; da Silva Duarte, J.L.; de Carvalho, S.H.V.; Soletti, J.I.; Meili, L. *Wodyetia bifurcata* biochar for methylene blue removal from aqueous matrix. *Bioresour. Technol.* **2019**, *293*, 122093. [\[CrossRef\]](#)
58. Ji, B.; Wang, J.; Song, H.; Chen, W. Removal of methylene blue from aqueous solutions using biochar derived from a fallen leaf by slow pyrolysis: Behavior and mechanism. *J. Environ. Chem. Eng.* **2019**, *7*, 103036. [\[CrossRef\]](#)
59. Esmaeili, H.; Foroutan, R. Adsorptive Behavior of Methylene Blue onto Sawdust of Sour Lemon, Date Palm, and Eucalyptus as Agricultural Wastes. *J. Dispers. Sci. Technol.* **2018**, *40*, 990–999. [\[CrossRef\]](#)
60. Wang, Y.; Zhang, Y.; Li, S.; Zhong, W.; Wei, W. Enhanced methylene blue adsorption onto activated reed-derived biochar by tannic acid. *J. Mol. Liq.* **2018**, *268*, 658–666. [\[CrossRef\]](#)

61. Pathania, D.; Sharma, S.; Singh, P. Removal of methylene blue by adsorption onto activated carbon developed from *Ficus carica* bast. *Arab. J. Chem.* **2017**, *10*, S1445–S1451. [[CrossRef](#)]
62. Suganya, S.; Kumar, P.S.; Saravanan, A.; Rajan, P.S.; Ravikumar, C. Computation of adsorption parameters for the removal of dye from wastewater by microwave assisted sawdust: Theoretical and experimental analysis. *Environ. Toxicol. Pharmacol.* **2017**, *50*, 45–57.
63. Su, Y.; Zhao, B.; Xiao, W.; Han, R. Adsorption behavior of light green anionic dye using cationic surfactant-modified wheat straw in batch and column mode. *Environ. Sci. Pollut. Res.* **2013**, *20*, 5558–5568. [[CrossRef](#)] [[PubMed](#)]
64. Mohan, D.; Sarswat, A.; Ok, Y.S.; Pittman, C.U., Jr. Organic and inorganic contaminants removal from water with biochar, a renewable, low cost and sustainable adsorbent—A critical review. *Bioresour. Technol.* **2014**, *160*, 191–202. [[CrossRef](#)] [[PubMed](#)]
65. Yi, S.; Gao, B.; Sun, Y.; Wu, J.; Shi, X.; Wu, B.; Hu, X. Removal of levofloxacin from aqueous solution using rice-husk and wood-chip biochars. *Chemosphere* **2016**, *150*, 694–701. [[CrossRef](#)]
66. Gong, H.; Zhao, L.; Rui, X.; Hu, J.; Zhu, N. A review of pristine and modified biochar immobilizing typical heavy metals in soil: Applications and challenges. *J. Hazard. Mater.* **2022**, *432*, 128668. [[CrossRef](#)]
67. Zhen, M.; Tang, J.; Song, B.; Liu, X. Decontamination of Methylene Blue from Aqueous Solution by Rhamnolipid-modified Biochar. *BioResources* **2018**, *13*, 3061–3081. [[CrossRef](#)]